line A_{mx}, so that the exact shift could not be ascertained.

It is interesting to compare the emission spectrum for $\mathbf{E}\perp c$ [Fig. 2(a)] and for the mixed-mode geometry [Fig. 2(b)]. In Fig. 2(a), the bound exciton lines (I, I', and I'') dominate the spectrum. Because a small component of the $\mathbf{E}$ vector can be resolved perpendicular to $\mathbf{k}$ in the mixed-mode geometry, the bound excitons should be observed in this geometry if they are also dipole-allowed transitions. The oscillator strengths of the bound excitons should depend upon ϕ, as given by Eq. (1). Also, because the reported refractive index[9] is larger near A_{mx} than the bound I lines, the refraction should be less near the I lines, so that these latter lines should consequently dominate the spectrum in Fig. 2(b). It is seen, however, that this is not the case. We believe that spatial dispersion effects may be responsible for the above unexpected behavior. It has been shown that the scattering of polaritons (apparent absorption) by phonons is dependent upon the shape of the polariton dispersion ($\mathbf{E}$ versus $\mathbf{k}$) curve.[10,11] Conversely, the contribution to the emission from the scattering of polaritons is expected to depend upon the shape of the dispersion curve especially just above the "knee" in the lower branch.[12] The knee occurs very near the crossing of the uncoupled exciton-photon dispersion curves, and it is at precisely this energy that the shape of the polariton dispersion curve is the most sensitive to the coupling parameter $4\pi\beta$. It may be expected, then, that the emission due to intrinsic excitons (polaritons) would have some implicit nonlinear dependence on $4\pi\beta_{mx}$, given by Eq. (1).[13]

In conclusion, emission lines have been observed in ZnO which clearly verify the existence of mixed-mode excitons in photoluminescence. Mixed-mode excitons are observed for the two lowest-lying excitons (A and B). This work points out the importance of precise alignment of uniaxial crystals when emission is measured for the polarization $\mathbf{E}\|c$, $\mathbf{k}\perp c$. It seems likely that a slight sample misalignment would account for the observations and polarization assignments recently reported for some of the emission lines in ZnO by Filinski and Skettrup.[7] Recent emission studies[7,14,15] have again pointed out the controversy over the valence-band assignments in ZnO suggested by Thomas[5] and by Park *et al.*[16] The observations made in this note are in agreement with the assignment of Thomas,[5] and because of the noted difference in behavior between intrinsic and extrinsic excitons, a further study may provide conclusive proof of intrinsic or extrinsic nature.

We wish to thank G. Voll for experimental assistance.

[9] Y. S. Park and J. R. Schenider, J. Appl. Phys. **39**, 3049 (1968).
[10] W. C. Tait and R. L. Weiher, Phys. Rev. **166**, 769 (1968).
[11] Y. Osaka, Y. Imai, and Y. Takeuti, J. Phys. Soc. Japan **24**, 236 (1968).
[12] W. C. Tait and R. L. Weiher, Phys. Rev. **178**, 1404 (1969).
[13] Mixed-mode excitons have also been observed in our laboratory in the emission spectrum of CdS crystals at different external angles ϕ'. The intensity of the "free" A exciton-mixed-mode line in CdS has a similar dependence on ϕ' as the A_{mx} line in ZnO.
[14] T. Skettrup and L. R. Lidholt, Solid State Commun. **6**, 589 (1968).
[15] C. Solbrig, Z. Physik **211**, 429 (1968).
[16] Y. S. Park, C. W. Litton, T. C. Collins, and D. C. Reynolds, Phys. Rev. **143**, 512 (1966).

PHYSICAL REVIEW VOLUME 185, NUMBER 3 15 SEPTEMBER 1969

Application of the Quantum-Defect Method to Optical Transitions Involving Deep Effective-Mass-Like Impurities in Semiconductors*

H. Barry Bebb
Texas Instruments Incorporated, Dallas, Texas 75222
(Received 27 January 1969; revised manuscript received 8 May 1969)

Approximate ground-state wave functions for effective-mass impurity centers of arbitrary binding energy are derived by the quantum-defect method and applied to calculate optical absorption and emission processes involving impurities in semiconductors. The dependences of band-impurity and impurity-ionization cross sections on impurity binding energy are calculated and shown to limit to those of the hydrogenic model and Lucovsky's δ-function model for shallow and deep impurity centers, respectively. Formulas relating the cross sections to the absorption coefficients and radiative recombination rates are also presented.

I. INTRODUCTION

THE observed binding energies of effective-mass impurities in semiconductors depend on the chemical species of the impurity ion (e.g., P, As, or Sb donors in silicon or germanium and B, Al, Ga, and In acceptors in silicon).[1] This is contrary to the simple effective-mass theory which predicts a unique binding energy (for all effective-mass impurities) that depends

* Work sponsored in part by U. S. Air Force Office of Scientific Research, under Contract No. F44620-67-C-0073.
[1] W. Kohn, in *Solid State Physics*, edited by F. Seitz and D. Turnbull (Academic Press Inc., New York, 1957), Vol. 5. Kohn briefly discusses the QDM (p. 289) in this connection, but because of an unfortunate error in his asymptotic wave function he does not attain the full significance of the formalism. Kohn records a hydrogenic function with the Bohr radius scaled to the observed energy in the usual way. The correct QD functions possess a rather different form and contain parameters which obviate the necessity of scaling quantities formally specified by the host-crystal properties, e.g., the effective Bohr radius.

only on host-crystal parameters such as dielectric constant and effective mass. Efforts to account for the observed chemical shifts have enjoyed limited success. An interesting treatment with references to earlier work is given by Morita and Nara.[2]

Because of the complexity of performing quasi-first-principles calculations, it is highly desirable to determine a simple means for obtaining good approximate wave functions which are sensitive to the impurity binding energy. The simplest means is, of course, to assume hydrogenic wave functions and scale the effective Bohr radius to reproduce the observed impurity binding energy $\epsilon(\text{obs})=-e^2/2Ka^*$. However, this procedure does not change the functional form of the wave functions but only their spatial extent; it requires assuming values of the effective mass m^* and dielectric constant K different from those appropriate to the host crystal; and, finally, it does not yield good agreement with empirical observation. Another approach to describe deep impurity centers was taken by Lucovsky.[3] He assumed the ion core of the impurity rather than the Coulomb potential arising from the impurity charge was responsible for the increased ground-state binding energy. He approximated the ion potential by a δ-function well and, borrowing from the deuteron photodissociation problem, determined simple wave functions to describe deep impurities. He applied the results to calculate the spectral dependence of the photo-ionization cross sections of impurities and achieved good agreement with the deep In center in silicon but not with the moderately deep Al and Sb acceptor impurities and certaintly not with the shallow B acceptor.

More recently, Bebb and Chapman[4] borrowed the well-known quantum-defect method (QDM) from atomic physics to calculate good approximate wave functions for impurity ions of arbitrary binding energy. Using QD functions to approximate both the ground state and continuum states of the impurity, the differing photo-ionization cross sections of B, Al, Sb, and In impurities in silicon as well as the Hg center in germanium were all accurately predicted. This successful test of the QD theory provides some confidence in its capability to provide accurate, but still simple, wave functions for impurity centers of arbitrary binding energy.

In the present work, QD functions are utilized to calculate rather general formulas for band-impurity absorption and recombination rates where the impurity centers can possess arbitrary binding energies. The results are compared with those obtained from the hydrogenic approximation in the limit of shallow impurities and Lucovsky's δ-function model in the limit of very deep impurities. In addition, the application of the QDM to impurity ionization is reexamined for the purpose of determining a simpler approximation to the positive-energy states than the continuum Coulomb functions used in Ref. 4. I find that "free waves" (or plane waves) appear to yield a far better approximation to the continuum states of impurity centers than could be expected from their rather poor showing in atomic calculations, e.g., photo-ionization of hydrogen or heavier alkali atoms.

While the major purpose of this paper is to apply the QDM to calculate optical cross sections involving impurities, the results are couched within a rather general discussion of absorption and emission processes in an attempt to simplify the application of the formulas to a wide range of experimental results. The band-edge value of the interband momentum matrix element p_{cv} as estimated from $\mathbf{k}\cdot\mathbf{p}$ perturbation theory is given for several typical band structures. Also, numerical values for factors containing atomic constants are recorded for convenience.

The regime of validity of the QDM as applied here corresponds to that of the general effective-mass theory for impurity centers, which finds application to a wide range of materials. Though most of the detailed work on deep effective-mass-like impurities has been restricted to those found in silicon and germanium, effective-mass theory is often applied to describe defect centers in III-V compounds, II-IV compounds, alkali halides, and more recently ferroelectric oxide crystals. The QDM of extending the effective-mass theory to deep impurities is applicable to a similar wide range of problems. Because of the broad scope envisioned, we restrict our attention to a presentation of theoretical results, with no attempt being made to explain any empirical data. The QDM has geen applied to the latter purpose in an earlier paper.[4]

II. QUANTUM-DEFECT THEORY

A. Bound States

The QDM is a standard and well-known technique in atomic physics and certain areas of solid-state physics. A general introductory discussion of the application of QDM to the impurity-ion problem, along with citations to the literature on the formal technique, is contained in Ref. 4. Only essential points are repeated here.

The QDM relies on the observation that while the impurity-induced potential energy is likely to be very complicated in the vicinity of the ion core, it must nevertheless, for large r, asymptotically approach a Coulomb potential $-e^2/Kr$. As has already been emphasized in connection with the δ-function model, the ion core can cause the binding energy of the impurity to differ greatly from that predicted by assuming a $1/r$ potential for all r. On the other hand, much of the wave function lies outside the core region, where the potential is given by $-e^2/Kr$. In this exterior region the wave functions are Coulombic; further, they must be continuous with the core function, which is unspecified. It is through the continuity requirement that the ex-

[2] A. Morita and H. Nora, J. Phys. Soc. Japan Suppl. 21, 234 (1966).
[3] G. Lucovsky, Solid State Commun. 3, 299 (1965).
[4] H. B. Bebb and R. A. Chapman, J. Phys. Chem. Solids 28, 2087 (1967).

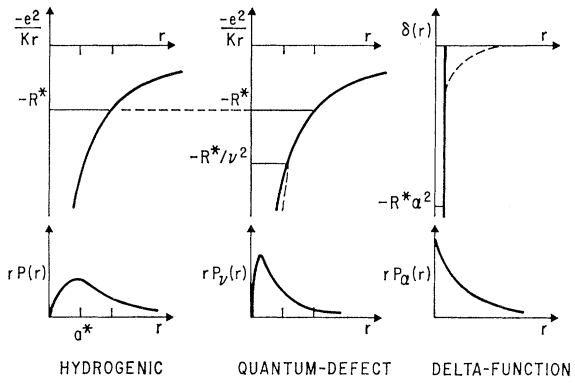

FIG. 1. Schematic of potentials and corresponding wave functions for different models (see text).

terior Coulomb function reflects the core potential. Since the core potential is unknown, we attempt to estimate its effect on the exterior region by looking for solutions of the wave equation with the eigenenergy replaced with the observed binding energy $\epsilon(\text{obs})$. In effect, the absence of knowledge about the potential in the core region is replaced by empirical information about the binding energy which is sensitive to the core.

The QD functions are solutions of

$$[-(\hbar^2/2m^*)\nabla^2-e^2/Kr-\epsilon(\text{obs})]F_\nu(r)=0, \quad (1)$$

which is valid in the region of large r. Since the observed energy $\epsilon(\text{obs})$ is not, in general, an eigenvalue of the differential equation, we cannot require the function to remain finite at the origin. However, divergence of the solution at $r=0$ does not affect its validity away from the origin, where the major contribution to optical integrals occurs. The general solution is a Whittaker function.[5] Specializing to the ground s state, we have

$$F_\nu(\mathbf{r})=P_\nu(r)Y_0^0(\theta,\phi). \quad (2)$$

The radial function can be approximated[4,5] by

$$P_\nu(r)=N_\nu r^{\nu-1}e^{-r/\nu a^*}, \quad (3a)$$

where

$$N_\nu=(2/\nu a^*)^\nu/(\nu a^*)^{1/2}\Gamma(\nu+1). \quad (3b)$$

The quantity ν is referred to as the effective principal quantum number. It is determined from the observed binding energy by

$$\epsilon(\text{obs})=-R^*/\nu^2, \quad (4)$$

where R^* is the hydrogenic Rydberg $e^2/2Ka^*$. This result is more familiar in the context of the alkali atoms. In the early days of atomic spectroscopy, it was noted that the emission-line energies of the alkali atoms were given by assuming

$$\epsilon_n(\text{obs})=-R^*/(n-\mu)^2, \quad (5)$$

where the parameter μ is called the quantum defect.

[5] M. J. Seaton, Monthly Notices Roy. Astron. Soc. 118, 504 (1958).

Its significance accrues from the fact that it remains nearly constant over a series of n values of a given angular momentum. Equations (4) and (5) imply the relation

$$\nu=n-\mu. \quad (6)$$

From the QD point of view, the wave functions are scaled from the binding energy in terms of ν rather than in terms of the effective-mass parameters a^* or R^*. Formally this is more acceptable, since a^* and R^* are, in principle, determined by host-crystal parameters, e.g., effective masses and dielectric constant, and should not be a function of the chemical species of the impurity. In applying the QDM, we obtain R^* as a solution of the effective-mass equation assuming a Coulomb potential $-e^2/Kr$. Deviations of the true potential $U(r)$ from a Coulomb potential in the core region are then taken into account by adjusting ν to reproduce the empirical binding energy.

It is instructive to compare the QD functions with the hydrogenic approximation in the limit of shallow impurities and the δ-function model in the limit of deep impurities. The hydrogenic wave function is given within the QD theory by setting $\nu=1$. Neglecting normalizations, the hydrogenic function in atomic units is

$$P_1(r)\sim e^{-r}; \quad (7a)$$

the QD function in atomic units is

$$P_\nu(r)\sim r^{\nu-1}e^{-r/\nu}, \quad (7b)$$

with ν given by $\epsilon(\text{obs})=-R^*/\nu^2$; and the δ-function-model wave function is[3]

$$P_\alpha(r)\sim r^{-1}e^{-\alpha r}, \quad (7c)$$

where $\alpha^2=-\epsilon(\text{obs})/R^*$. Clearly, ν and α are reciprocally related: $\alpha=\nu^{-1}$. For very deep centers, ν is small and the factor r^ν in (7b) becomes slowly varying over the range of r where $P_\nu(r)$ is significant. Consequently, in the limit of small ν (large binding energies), the function (7c) yields a good approximation to the QD function (7b), i.e.,

$$P_\nu(r) \underset{\nu\to 0}{\sim} r^{-1}e^{-r/\nu}.$$

It appears that the QD function essentially contains both the hydrogenic approximation and the δ-function model as limiting cases but is also valid in the region of intermediate binding energies.

Figure 1 compares $rP(r)$ together with corresponding potentials for the three models. As the binding energy increases from the hydrogenic value R^* (and ν decreases), the QD function becomes more compact, with the charge distribution $r^2|P_\nu(r)|^2dr$ increasing rapidly near the core. This is just the behavior that should have been expected from our earlier arguments connecting the binding energy and the core potential. All three wave functions, of course, become more compact with increasing binding energies, but their behavior

for large r differs depending on the parameters a^*, ν, or α, respectively.

B. Continuum States

Quantum-defect Coulomb functions can also be obtained as solutions of Eq. (1) for the positive energy states. These continuum Coulomb functions were utilized as the final-state functions for calculating the photo-ionization cross section in Ref. 4. However, the positive-energy Coulomb functions are rather intractable; in addition, their use involves the complication of estimating the QD parameter μ appropriate to the continuum. While, in principle, the QD for the continuum states can be extrapolated from the higher-lying bound states, the procedure is so imprecise that, for most practical purposes, μ remains an adjustable parameter.

Here we consider the simpler approximation of plane-wave continuum functions. These functions are considerably easier to use for computations and lead to analytical functions for the required dipole matrix elements. It would not be readily expected that plane-wave functions should be as good an approximation to the positive-energy solutions of Eq. (1) as the Coulomb functions used in Ref. 4. However, contrary to expectations, appeal to experiment indicates they often provide an excellent approximation. In the next few paragraphs we present the free-wave solutions followed by an attempt to rationalize their use.

Free-wave functions are obtained as solutions of Eq. (1) with the Coulomb potential put equal to zero, e.g., let $e^2/K \rightarrow 0$. The resulting equation,

$$[-(\hbar^2/2m^*)\nabla^2 - \epsilon(\text{obs})]F(r)=0, \tag{8}$$

can be diagonalized simultaneously in energy H and momentum $\mathbf{p}$ (Cartesian coordinates x, y, z) to yield plane waves $e^{i\mathbf{k}\cdot\mathbf{r}}$, or it can be diagonalized simultaneously in energy H, angular momentum $|\mathbf{L}|^2$, and z projection of the angular momentum L_z (spherical coordinates) to yield functions formed from products of spherical Bessel functions $j_l(kr)$ and spherical harmonics $Y_l^m(\theta,\phi)$, i.e., $j_l(kr)Y_l^m(\theta,\phi)$. Since both sets of functions form complete sets, one can be expanded into the other. The well-known expansion[6]

$$e^{i\mathbf{k}\cdot\mathbf{r}}=4\pi\sum_{l=0}^{\infty}\sum_{m=-l}^{l} i^l j_l(kr)Y_l^m(\theta,\phi)Y_l^{m*}(\hat{k}) \tag{9}$$

is of computational use. The second spherical harmonic $Y_l^m(\hat{k})$ depends on $\mathbf{k}$. It is a function of the arguments (θ_k,ϕ_k) specifying the direction of the unit vector $\hat{k}$. We shall utilize this expansion in calculating both band-impurity transitions and impurity-ionization and capture processes.

In atomic physics, for example, in calculating photoionization cross sections of the hydrogen atom, free-wave functions do not provide a good approximation except in the high-energy limit. Why, then, do free waves appear to be adequate for calculating photoionization cross sections of impurities in semiconductors, as indeed we will later establish to be true?

It is possible to speculate that the larger orbits associated with the excited discrete and continuum p states are shielded from the core potential of the impurity ion, while at the same time the more compact ground-state s function (which is finite at $r=0$) experiences the full core potential. In fact, the higher-energy bound p states of the deeper group-III impurities in silicon do show some tendency to become more weakly bound than predicted from a Coulomb potential. This trend leads to the use of negative QD parameters in the continuum, which in turn forces the Coulomb waves to approach free waves more closely.

Additional support for our speculation is provided by the success of Lucovsky's δ-function model for describing deep centers.[3,7,8] As previously discussed, the binding energy of the ground-state s function is largely determined by the short-range ion core potential. If the potential is assumed to be a δ function, no excited bound states occur, and the continuum states are free-wave Bessel functions. Adding weak "Coulomb-like tails" to the δ-function core potential will introduce bound excited states and cause some distortion of the continuum states. If the Coulomb tails do not extend over a range that is too great, the distortion of the continuum states may not be significant.

III. ABSORPTION AND EMISSION PROCESSES

The formulas for the absorption coefficient and the spontaneous recombination rate involve the transition rate between individual states, the number of filled initial states, and the number of empty final states. The number of filled or empty states is given by the total number of states times the occupational probability (e.g., Fermi-Dirac, Boltzmann, etc.). The manner in which the number of states enters depends, among other things, on whether or not the probability of the state being filled or empty is dependent or independent of the occupation of the other states. Consider two energy levels E_u and E_l, formed from N_u and N_l states. Let $n_l=N_l f_l$ and $n_u'=N_u f_u'$ be the number of occupied lower and empty upper states, respectively. If the occupation probability of the lower states f_l is independent of the occupation of the upper states f_u', and all $N_u N_l$ states are coupled by optical transitions, then the optical transition rate from E_u to E_l must be proportional to $n_u n_l'$. This product enters in a natural way upon summing over all initial and final states

[6] A. Messiah, *Quantum Mechanics* (John Wiley & Sons, Inc., New York, 1962), Vol. I, p. 359.

[7] R. A. Chapman and W. G. Hutchinson, Phys. Rev. **157**, 615 (1967).

[8] J. S. Blakemore, Phys. Rev. **173**, 767 (1968).

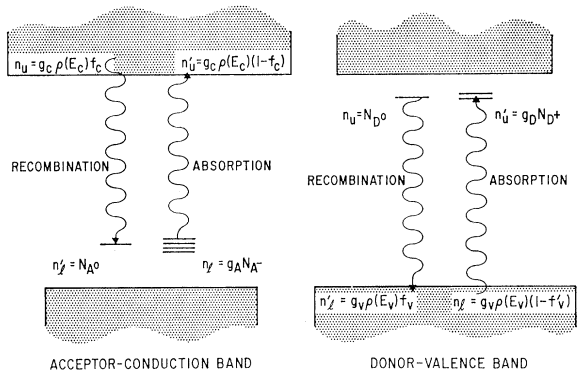

FIG. 2. Band-impurity absorption and recombination showing the difference in the effective degeneracy for neutral and ionized impurities. Donor is illustrated as twofold-degenerate (spin degeneracy) and acceptor is illustrated as fourfold-degenerate (two degenerate valence bands plus spin degeneracy).

appearing in the transition rate, say, as calculated from Fermi's "Golden rule":

$$\mathcal{W}=\frac{2\pi}{\hbar}\sum_{u,l}|\mathcal{H}_{ul}|^2\delta(E_{ul}-\hbar\omega). \tag{10}$$

Similarly, the number of downward transitions is proportional to $n_l n_u'$. Clearly, the interaction Hamiltonian $\mathcal{H}_{ul}$ may contain selection rules (e.g., spin flips are forbidden) that eliminate some of the terms but still leave the transition rate proportional to the product $N_u N_l$. With these assertions, the absorption coefficient (in units of cm^{-1}) follows directly from the Golden rule:

$$\alpha(\hbar\omega)=\frac{2\pi}{\hbar V_{EN}(\hbar\omega)}\sum_{Eu,El}\langle|\mathcal{H}_{ul}|^2\rangle_{av}\times(n_l n_u'-n_u n_l')\delta(E_{ul}-\hbar\omega). \tag{11}$$

The spontaneous emission rate is somewhat more difficult to derive but can be shown to be

$$R_{SP}(\hbar\omega)=\frac{2\pi}{\hbar}G(\hbar\omega)\sum_{Eu,El}\langle|\mathcal{H}_{ul}|^2\rangle_{av}\times n_u n_l'\delta(E_{ul}-\hbar\omega). \tag{12}$$

The sums over E_u and E_l account for the fact that more than one pair of energy levels can conserve energy with $\hbar\omega$. In these formulas, $V_{EN}(\hbar\omega)$ is the radiation-field-energy velocity; it is related to the index of refraction $n(\hbar\omega)$ through the real part of the dielectric constant by $\epsilon_r V_{EN}(\hbar\omega)=n(\hbar\omega)c$.[9] The optical density of states is

$$G(\hbar\omega)=\frac{n^2(\hbar\omega)(\hbar\omega)^2}{(\pi c)^2\hbar^3 V_G}, \tag{13}$$

where V_G is the group velocity. The "reduced" interaction Hamiltonian $|\mathcal{H}_{ul}|^2$ is defined as the energy of interaction for one photon[10]:

$$|\mathcal{H}_{ul}|^2=\frac{2\pi e^2\hbar\omega}{\epsilon_r m^2\omega^2}|\langle u|e^{-i\mathbf{k}_\lambda\cdot\mathbf{r}}\hat{\epsilon}_\lambda\cdot\mathbf{p}|l\rangle|^2, \tag{14}$$

where $\mathbf{k}_\lambda$ is the wave vector of the radition field and $\hat{\epsilon}_\lambda$ is the polarization direction, which we will normally take as z. The angular brackets around the matrix element in Eqs. (11) and (12) indicate an average over all degenerate initial and final states appearing in (14). In the standard dipole approximation, we have $e^{-i\mathbf{k}\cdot\mathbf{r}}\simeq 1$. For most cases of interest to semiconductor physics, the energy summations in Eqs. (11) and (12) are eliminated. One summation is of course eliminated by the energy-conserving δ function $\delta(E_{ul}-\hbar\omega)$. The disposition of the remaining summation depends on the particular case of interest. For band-to-band transitions, momentum conservation does the trick. For transitions involving impurities, the discreteness of the impurity state provides the second δ function needed. Since this is the case of interest here, we will treat it explicitly. Let the lower level be a discrete impurity state at energy (E_I): then we have

$$n_l=n_l(E_l)\delta(E_l-E_I) \tag{15}$$

and

$$n_l'=n_l'(E_l)\delta(E_l-E_I). \tag{16}$$

Substituting into Eqs. (11) and (12) eliminates the sums over E_u and E_l through the agency of the δ functions:

$$\int dE_u dE_l\delta(E_{ul}-\hbar\omega)\delta(E_l-E_I). \tag{17}$$

Clearly, the same result obtains if the impurity is the upper level; hence, (11) and (12) reduce to

$$\alpha(\hbar\omega)=\frac{2\pi}{\hbar V_{EN}(\hbar\omega)}\langle|\mathcal{H}_{ul}|^2\rangle_{av}(n_l n_u'-n_u n_l') \tag{18}$$

and

$$R_{SP}(\hbar\omega)=\frac{2\pi}{\hbar}G(\hbar\omega)\langle|\mathcal{H}_{ul}|^2\rangle_{av}n_u n_l'. \tag{19}$$

From Eq. (18), the absorption cross section $\sigma(\hbar\omega)$ (in units of cm^2) is defined in the standard way:

$$\sigma(\hbar\omega)=\frac{2\pi}{\hbar V_{EN}(\hbar\omega)}\langle|\mathcal{H}_{ul}|^2\rangle_{av}\rho(E_j), \quad j=u,l \tag{20}$$

where $\rho(E_j)$ is the density of continuum states. In terms of $\sigma(\hbar\omega)$, we have

$$\alpha(\hbar\omega)=\sigma(\hbar\omega)(n_l n_u'-n_u n_l')/\rho(E_j) \tag{21}$$

and

$$R_{SP}(\hbar\omega)=\sigma(\hbar\omega)V_{EN}(\hbar\omega)G(\hbar\omega)n_u n_l'/\rho(E_j), \tag{22}$$

[9] R. S. Knox, in *Solid State Physics*, edited by F. Seitz and D. Turnbull (Academic Press, Inc., New York, 1963), Suppl. 5, p. 105.

[10] W. Heitler, *The Quantum Theory of Radiation* (Oxford University Press, London, 1957), p. 176.

where $j=u$, l, depending on whether the continuum level is the upper or lower energy level. These formulas readily reveal the relation between $\alpha(\hbar\omega)$ and $R_{SP}(\hbar\omega)$ as determined from detailed balancing.[11]

The absorption cross section defined above contains the information pertaining to the transition probability between one filled and one empty state. Using the relation[9] $\epsilon_r V_{EN}(\hbar\omega)=n(\hbar\omega)c$, in combining Eqs. (14) and (20) gives for the cross section

$$\sigma(\hbar\omega)=\frac{4\pi^2\alpha_0\hbar\omega}{n(\hbar\omega)}\frac{\langle|p_{ul}|^2\rangle_{av}}{m^2\omega^2}\rho(E), \tag{23}$$

where $\rho(E)$ is the density of final states and α_0 is the fine-structure constant $e^2/\hbar c$. The momentum matrix element is averaged over all degenerate states. Let g_u and g_l denote the degeneracies of the energy levels E_u and E_l; then

$$\langle|p_{ul}|^2\rangle_{av}=\frac{1}{g_u g_l}\sum_{d_u d_l=1}^{g_u g_l}|p_{ul}|^2. \tag{24}$$

If only spin degeneracy occurs and spin flips are forbidden, then we have

$$\langle|p_{ul}|^2\rangle_{av}=\tfrac{1}{2}|p_{ul}|^2. \tag{25}$$

Averages over degenerate impurity states arising from multiple bands (e.g., complex valence-band structure of most elemental and compound semiconductors) usually do not introduce additional factors. Thus the general average in Eq. (24) often reduces to (25).

In the following sections we calculate the cross sections for band-impurity transitions of the type shown in Fig. 2 and impurity-ionization (and capture) processes illustrated in Fig. 3. Considering both processes in juxtaposition provides an opportunity to contrast certain aspects of the two calculations. Band-impurity (e.g., donor–valence-band or acceptor–conduction-band) transitions are adequately described as transitions between a bound impurity state and a band Bloch function. In contrast, photo-ionization reduces to a calculation between localized impurity states, namely, between the discrete negative-energy ground state and the continuum positive-energy excited state (in exact analogy with photo-ionization of the hydrogen atom). In order to distinguish the impurity-induced positive-energy continuum states from the Bloch functions, we refer to localized continuum states in Fig. 3. Localization is something of a misnomer, but it nevertheless retains a certain precision in suggesting the formal commonality of the negative- and positive-energy solutions of the effective-mass equation (1).

IV. BAND-IMPURITY CROSS SECTION

A. Spectral Shape

Consider optical transitions between the conduction band and an acceptor contained in a semiconductor

[11] E. W. Williams and H. B. Bebb, J. Phys. Chem. Solids **30**, 1289 (1969).

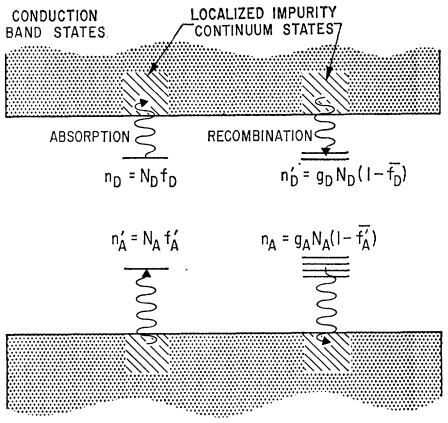

FIG. 3. Impurity-ionization and capture processes illustrating difference in the effective degeneracy for neutral and ionized impurities. Donor is illustrated as twofold-degenerate and acceptor as fourfold-degenerate.

possessing simple parabolic bands with only spin degeneracy (see Fig. 2). In the simplest approximation, the acceptor wave function is given as a product of the valence-band Bloch function at the band edge—say, $k=0$—and the slowly varying envelope function obtained as a solution to Eq. (1)[1]:

$$|A\rangle=F_\nu(\mathbf{r})u_{v,0}(\mathbf{r})=|\nu;v,0\rangle. \tag{26}$$

The conduction band is described by the usual Bloch function

$$|c,\mathbf{k}\rangle=e^{i\mathbf{k}\cdot\mathbf{r}}u_{c,\mathbf{k}}(\mathbf{r}). \tag{27}$$

In a well-known approximation,[1] valid when $F_\nu(\mathbf{r})$ is slowly varying compared to the periodicity of $u_{n,\mathbf{k}}(\mathbf{r})$, the momentum matrix element reduces to

$$\langle c,\mathbf{k}|p_z|\nu;v,0\rangle=p_{cv}(\mathbf{k})a_\nu(\mathbf{k}), \tag{28}$$

where

$$a_\nu(\mathbf{k})=\int_0^\infty e^{-i\mathbf{k}\cdot\mathbf{r}}F_\nu(\mathbf{r})d\tau \tag{29}$$

and $p_{cv}(\mathbf{k})$ is the usual momentum matrix element between the conduction and valence bands. In all cases examined by $\mathbf{k}\cdot\mathbf{p}$ calculations, it is found that $p_{cv}(\mathbf{k})$ can be replaced quite accurately by the band-edge value $p_{cv}(0)$.[12] This, of course, is a standard approximation, but we wish also to stress that it is a good approximation even when band warping is appreciable.

From the partial-wave expansion (9) we have

$$a_\nu(\mathbf{k})=4\pi\sum_{l=0}\sum_{m=-l}^{l}(-i)^l Y_l^m(\hat{k})\int j_l(kr)P_\nu(r)r^2dr \times\int Y_l^{m*}(\theta,\phi)Y_0^0(\theta,\phi)d\Omega. \tag{30}$$

Evaluating the angular integral (noting the usual selec-

[12] E. O. Kane, J. Phys. Chem. Solids **1**, 249 (1957).

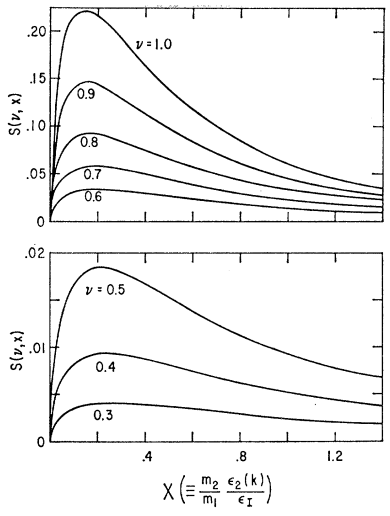

FIG. 4. Plot of shape function $S(\nu,x)$ versus normalized energy x for several values of ν. The normalization is chosen so that in the hydrogenic limit $S(1,x)$ reduces to the function $x^{1/2}/(1+x)^4$ defined by Eagles. The absorption cross section is proportional to $S(\nu,x)$. The decreasing magnitude and weaker spectral dependence makes experimental observation of the deeper centers more difficult.

tion rules) and substituting in the defining relations for $j_0(kr)=\sin(kr)/kr$ and $P_\nu(r)=N_\nu r^{\nu-1}e^{-r/\nu a^*}$, we have

$$a_\nu(\mathbf{k})=4\pi N_\nu k^{-1}Y_0{}^0(\hat{k})a^{*\nu+2}\int \rho^\nu \sin(k'\rho)\, e^{-\rho/\nu}d\rho, \quad (31)$$

where $\rho=r/a^*$ and $k'=ka^*$. The integral is evaluated in the Appendix. Noting also that $Y_0{}^0(\hat{k})=(4\pi)^{-1/2}$, we finally obtain

$$|a_\nu(k)|^2=\frac{4\pi 2^{2\nu}(\nu a^*)^3\sin^2(\nu+1)\tan^{-1}(\nu ka^*)}{(\nu ka^*)^2[1+(\nu ka^*)^2]^{\nu+1}}. \quad (32)$$

In the hydrogenic limit, $\nu=1$ and (32) reduces to the familiar form[13,14]

$$|a_{\nu=1}(k)|^2=64\pi a^{*3}/[1+(ka^*)^2]^4. \quad (33)$$

For the opposite limit of very deep impurity centers, the δ-function model yields

$$|a_\alpha(k)|^2=8\pi(a^*/\alpha)^3/[1+(ka^*/\alpha)^2]^2, \quad (34)$$

where $\alpha^2=-\epsilon(\text{obs})/R^*$.

It is this expression for $|a(k)|^2$ that reflects the use of different approximations for the wave function. All three expressions (32)–(34) show the same qualitative behavior, namely, that $a(k)$ remains nearly constant for k out to some value reciprocally related to the extent of the impurity envelope function—say, in the QD case, $k\sim 1/\nu a^*$. Indeed, the integral (29) defining $a_\nu(\mathbf{k})$ is in reality just the Fourier transform of $F_\nu(\mathbf{r})$. As ν becomes smaller corresponding to increased binding energies, the wave function becomes increasingly compact, and larger values of $\mathbf{k}$ space are requird to represent $F_\nu(\mathbf{r})$. This same Fourier relationship also exists in other approximations, e.g., scaled hydrogenic or δ-function-model wave functions. Consequently, the QD results differ quantitatively but not qualitatively from other theories; arguments based on Fourier relationships would seem to preclude any great differences from being introduced by any theory. However, the distinction between quantitative and qualitative depends on the measurement scale. From the experimental measuring stick of data interpretation, changes introduced into the predicted optical properties by the QD model are substantial.

In order to investigate in more detail how QD formulas differ from hydrogenic formulas, it is useful to cast the results into a slightly different form. Still referring explicitly to acceptor–conduction-band transitions, we can write the cross section using Eq. (23) as,

$$\sigma(\hbar\omega)=\frac{\alpha_0\hbar\omega}{n(\hbar\omega)}\frac{1}{2}\frac{|p_{cA}|^2}{m^2\omega^2}\delta_c\left(\frac{2m_c}{\hbar^2}\right)^{3/2}\epsilon_c{}^{1/2}, \quad (35)$$

where the conduction-band density of states is (not including spin)

$$\rho(E_c)=\frac{\delta_c}{(2\pi)^2}\left(\frac{2m_c}{\hbar^2}\right)^{3/2}\epsilon_c{}^{1/2}, \quad (36)$$

where δ_c is a factor differing from unity only if the conduction mass is not a constant (nonparabolic bands), and where m_c is the band-edge value of the mass. Defining

$$x_c=m_c\epsilon_c/m_v\epsilon_A,$$

where (37)

$$\epsilon_c=\hbar^2k^2/2m_c=\hbar\omega-\epsilon_G-\epsilon_A,$$

we can write the cross section [upon substituting $|p_{cA}|^2=|p_{cv}|^2|a_\nu(k)|^2$]

$$\sigma(\hbar\omega)=\frac{2^5\alpha_0}{n(\hbar\omega)}\frac{|p_{cv}|^2}{m^2\omega^2}\frac{m_c\hbar\omega}{m_vR_v^*}\delta_cS(\nu,x_c), \quad (38)$$

where R_v^* is the effective Rydberg appropriate to the valence-band mass m_v, and where

$$S(\nu,x_c)=\frac{\nu^2 2^{2\nu}\sin^2(\nu+1)\tan^{-1}(x_c{}^{1/2})}{16x_c{}^{1/2}(1+x_c)^{\nu+1}}. \quad (39)$$

Here we have also identified $\nu^2k^2a_v{}^{*2}=m_c\epsilon_c/m_v\epsilon_A=x_c$. The dependence of the cross section on impurity binding energy [$\epsilon_A(\text{obs})=R_v^*/\nu^2$] is contained entirely in the shape function $S(\nu,x_c)$. For $\nu=1$, $S(1,x_c)$ reduces to the function $x_c{}^{1/2}/(1+x_c)^4$ defined by Eagles.[13] In the δ-function limit we have $S(\alpha,x_c)=(1/8\alpha^2)x_c{}^{1/2}/(1+x_c)^2$.

[13] D. M. Eagles, J. Phys. Chem. Solids **16**, 76 (1960).
[14] W. P. Dumke, Phys. Rev. **132**, 1998 (1963).

Figure 4 plots $S(\nu,x)$ for several values of ν. For generality the masses are identified by numerical subscripts, with 1 referring to the band coupled with the impurity ion and 2 referring to the opposite band. Two features are apparent. First is the decreasing magnitude of $S(\nu,x)$ with decreasing ν, and second is the apparent weaker spectral dependence. As remarked above, these qualitative features should occur in any approximation. The quantitative differences in $S(\nu,x)$ for different values of ν are made more apparent by plotting $S(\nu,x)/S_{\max}$ in Fig. 5. On this plot the hydrogenic approximation ($\nu=1$) yields a unique spectral curve for all choices of the effective Bohr radius. The changes in $S(\nu,x)/S_{\max}$ as a function of ν are peculiar to the QD theory. At the opposite limit of infinite binding indicated by $\nu\rightarrow 0.0$ and calculated using δ-function-model wave functions, we also obtain an invariant curve. The QD model spans the region between, as well as incorporating, the two limits.

A formula describing the cross section for valence-band-to-donor transitions is obtained from Eq. (38) by interchanging c and v and replacing ϵ_A by ϵ_D. Thus, in general, we can write for band-impurity transitions

$$\sigma(\hbar\omega)=\frac{2^5\pi\alpha_0}{n(\hbar\omega)}\frac{|p_{cv}|^2}{m^2\omega^2}\frac{m_2\hbar\omega}{m_1R_1^*}\delta_2S(\nu,x_2), \tag{40}$$

where $x_2=m_2\epsilon_2/m_1\epsilon_1$. For donor–valence-band transitions, we have $2\rightarrow v$ and $1\rightarrow c$, and for acceptor–conduction-band transitions, we have $2\rightarrow c$ and $1\rightarrow v$.

B. Magnitude

For certain well-known band structures the momentum matrix element can easily be evaluated from $\mathbf{k}\cdot\mathbf{p}$ perturbation theory as applied by Kane. We consider first the band structure appropriate to direct-gap III-V compounds, i.e., a spin-degenerate conduction band separated by ϵ_G from a valence-band structure formed from spin-degenerate light- and heavy-hole bands degenerate at $\mathbf{k}=0$ and a split-off band separated by the energy Δ.[15] From the f-sum rule,[16] the conduction-band mass at $k=0$ is

$$\frac{1}{m_c}=\frac{1}{m}+\frac{2}{m^2}\sum_{v=h,l,s}\frac{|p_{cv}|^2}{E_c(0)-E_v(0)}, \tag{41}$$

where

$$\begin{aligned}E_c(0)-E_v(0)&=\epsilon_G, \quad \text{for } v=h,l\\ &=\epsilon_G+\Delta, \quad \text{for } v=s.\end{aligned} \tag{42}$$

From Kane's calculations it can be shown that[12,14,17]

$$|p_{ch}|^2=p_{cl}|^2=|p_{cs}|^2; \tag{43}$$

[15] E. J. Johnson, *Semiconductors and Semimetals* (Academic Press Inc., New York, 1967), Vol. III, p. 153.
[16] A. H. Wilson, *The Theory of Metals* (Cambridge University Press, Cambridge, England, 1953), 2nd ed.
[17] F. Stern, in *Solid State Physics*, edited by F. Seitz and D. Turnbull (Academic Press Inc., New York, 1963), Vol. 15, p. 370.

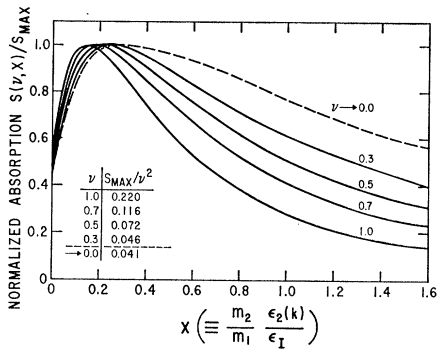

FIG. 5. Plot of normalized shape function $S(\nu,x)/S_{\max}$ versus normalized energy x. The dashed curve indicated by $\nu\rightarrow 0.0$ is obtained from the δ-function model (see text).

then we have

$$|p_{cv}|^2=\frac{\epsilon_Gm^2}{6\bar{m}_c}\frac{\epsilon_G+\Delta}{\epsilon_G+\frac{2}{3}\Delta}, \tag{44}$$

where $\bar{m}_c$ is the mass parameter introduced by Kane.[18] It is related to the effective mass m_c through

$$m/\bar{m}_c=m/m_c-1. \tag{45}$$

In most instances, we have $\epsilon_G\gg\Delta$, making $\epsilon_Gm^2/6\bar{m}_c$ a good approximation to $|p_{cv}|^2$. By trivial rearrangement we can also write other useful computational formulas:

$$\frac{|p_{cv}|^2}{m^2\omega^2}=\frac{\epsilon_G}{6\bar{m}_c\omega^2}=\frac{\epsilon_GR_1^*}{3(\hbar\omega)^2}\frac{m_1}{\bar{m}_c}a_1^{*2}, \tag{46}$$

where 1 refers to the band associated with the impurity.

Combining Eqs. (40) and (46) gives

$$\sigma(\hbar\omega)=\frac{2^5\pi\alpha_0a_1^{*2}}{3n(\hbar\omega)}\frac{\epsilon_G}{\hbar\omega}\frac{m_2}{\bar{m}_c}\delta_2S(\nu,x_2). \tag{47}$$

The quantity $\frac{4}{3}\pi\alpha_0a_0^2$ is common to many cross-section calculations and has the value 8.56×10^{-19} cm^2. Inserting this value gives

$$\sigma(\hbar\omega)=\frac{8(a_1^*/a^0)^2}{n(\hbar\omega)}(8.56\times10^{-19})\frac{\epsilon_Gm_2}{\hbar\omega\bar{m}_c}\delta_2S(\nu,x_2)\text{ cm}^2. \tag{48}$$

For donor–valence-band transitions, both the light- and heavy-hole bands can contribute (and perhaps the split-off band also). Then the cross section is obtained by summing over the valence bands[14]:

$$\sigma(\hbar\omega)=\frac{8(a_1^*/a_0)^2}{n(\hbar\omega)}(8.56\times10^{-19})\times\frac{\epsilon_G}{\hbar\omega\bar{m}_c}\sum_v m_v\delta_vS(\nu,x_v)\text{ cm}^2. \tag{49}$$

Other examples are readily worked out from the f sum rule. Particularly simple is the two-band model

[18] See, for example, Eqs. (49) and (68) of Ref. 15.

with $|p_{cv}|^2$ given by

$$\frac{1}{m_c}=\frac{1}{m}+\frac{2}{m^2}\frac{|p_{cv}|^2}{\epsilon_G}, \tag{50}$$

or

$$|p_{cv}|^2=\epsilon_G m^2/2\bar{m}_c, \tag{51}$$

which compares with Eq. (44).

Equation (51) can also be used to estimate $|p_{cv}|^2$ for more complex band structures upon dividing by the number of contributing degenerate (or nearly degenerate) bands summed on in the f sum rule. This rule is easily verified directly from Eq. (41).[19]

V. PHOTO-IONIZATION CROSS SECTION

Photo-ionization and radiative capture involve transitions between states made up from a given band (i.e., donors associated with the conduction band and acceptors with the valence band).[4] Thus it is not necessary to distinguish between bands with the same care as when different bands are involved. Associating the impurity level with a band of index b gives the ground-state s function of the impurity as a product of the envelope function $F_\nu(\mathbf{r})$ and the band-edge Bloch function $u_{b,0}(\mathbf{r})$:

$$|I\rangle=F_\nu(\mathbf{r})u_{b,0}(\mathbf{r}). \tag{52}$$

Similarly, the continuum state is given by a plane-wave "envelope function" $e^{i\mathbf{k}\cdot\mathbf{r}}$ multiplied by $u_{b,0}(\mathbf{r})$:

$$|I'\rangle=e^{i\mathbf{k}\cdot\mathbf{r}}u_{b,0}(\mathbf{r}). \tag{53}$$

In calculating intraimpurity transitions it is more convenient to use the dipole moment operator z than the momentum operator p_z. Again with the standard approximation that the envelope functions are slowly varying with respect to the periodicity of the Bloch functions, the dipole integral reduces to

$$\langle I'|z|I\rangle=\int e^{-i\mathbf{k}\cdot\mathbf{r}}zF_\nu(\mathbf{r})d\tau. \tag{54}$$

Because of the appearance of $\cos\theta$ from $z=r\cos\theta$, only the p-wave term in the partial-wave expansion (9) survives:

$$\begin{aligned}\langle I'|z|I\rangle&=-i4\pi Y_1^0(\hat{k})\int Y_1^0\cos\theta\, Y_0^0 d\Omega\\ &\quad\times\int j_1(kr)rP_\nu(r)r^2dr\\ &=-\frac{4\pi}{\sqrt{3}}Y_1^0(\hat{k})N_\nu\int j_1(kr)r^{\nu+2}e^{-r/\nu}dr,\end{aligned} \tag{55}$$

where the second line follows upon performing the angular integral. The $l=1$ spherical Bessel function is $j_1(kr)=\sin(kr)/(kr)^2-\cos(kr)/kr$. Performing the integral over r gives

$$|\langle I'|z|I\rangle|^2=\tfrac{1}{3}(4\pi)^2|Y_1^0(\hat{k})|^2\frac{(\nu a^*)^5}{y}\frac{\nu 2^{2\nu}}{(1+y)^{\nu+1}}f(y), \tag{56a}$$

where

$$f(y)=\left(\frac{\sin(\nu+1)\tan^{-1}(y^{1/2})}{y^{1/2}}-\frac{(\nu+1)\cos(\nu+1)\tan^{-1}(y^{1/2})}{(1+y)^{1/2}}\right)^2 \tag{56b}$$

and

$$y=(\nu ka^*)^2=\epsilon_b/\epsilon_I=(\hbar\omega-\epsilon_I)/\epsilon_I. \tag{56c}$$

The last identity follows trivially from the definition of ϵ_b:

$$\epsilon_b=\hbar^2k^2/2m_b=R_b^*(ka^*)^2=\epsilon_I(\nu ka^*)^2. \tag{56d}$$

Finally, we must average the matrix element over all degenerate initial and final states. The average over final states includes an average over the possible directions of $\hat{k}$ [namely, $\int|Y_1^0(\hat{k})|^2(d\Omega_k/4\pi)=(4\pi)^{-1}$], as well as over the spin and band degeneracies. Substituting the result into Eq. (23) and recalling that $|p_{ul}|^2=m^2\omega_{ul}^2|z_{ul}|^2$, we obtain

$$\begin{aligned}\sigma(\hbar\omega)&=\frac{4\pi^2\alpha_0\hbar\omega}{n(\hbar\omega)}\langle|\langle I'|z|I\rangle|^2\rangle_{\text{av}}\frac{1}{(2\pi)^2}\left(\frac{2m_b}{\hbar^2}\right)^{3/2}\epsilon_b^{1/2}\\ &=\frac{\alpha_0(1+y)}{n(\hbar\omega)(\nu a^*)^3}\langle|\langle I'|z|I\rangle|^2\rangle_{\text{av}}y^{1/2}\\ &=\frac{4\pi\alpha_0a^{*2}}{3n(\hbar\omega)}(1+y)\frac{1}{2}\frac{\nu^3 2^{2\nu}f(y)}{y^{1/2}(1+y)^{\nu+1}},\end{aligned} \tag{57}$$

where $y=(\hbar\omega-\epsilon_I)/\epsilon_I$ and $f(y)$ is given by Eq. (56b). Again numerically evaluating $4\pi\alpha_0a_0^2/3=8.56\times10^{-19}$ cm^2 and defining the normalized matrix element corresponding to Ref. 4

$$|g|^2=\frac{\nu 2^{2\nu}f(y)}{y^{1/2}(1+y)^{\nu+1}}, \tag{58}$$

we obtain

$$\begin{aligned}2\sigma(\hbar\omega)&=\frac{(a^*/a_0)^2}{n(\hbar\omega)}(8.56\times10^{-19})\nu^2(1+y)|g|^2\text{ cm}^2\\ &=\frac{(a^*/a_0)^2}{n(\hbar\omega)}a(\hbar\omega).\end{aligned} \tag{59}$$

The factor of 2 appearing with $\sigma(\hbar\omega)$ arises from the average over spins, assuming that spin flips are forbidden. Often the spin degeneracy is included in the density of final states and cancels the $\frac{1}{2}$ arising from the average over spins. However, here we chose to maintain

[19] O. Madelung [*Physics of III-V Compounds* (John Wiley & Sons, Inc., New York, 1964)] gives a useful discussion of the relation of $|p_{cv}|^2$ to the effective masses.

all degeneracy factors explicitly in the number of initial and final states, i.e., $\sigma(\hbar\omega)$ is the cross section appropriate to one "average" initial state and one "average" final state.

Figure 6 presents the normalized atomic cross section $a(\hbar\omega)/\nu^2$ versus the normalized photon energy $\hbar\omega/\epsilon_I$ for several values of ν. Lucovsky's δ-function model was used to calculate the $\nu \rightarrow 0.0$ curve. From the figure there is a clear trend starting at the $\nu=1$ curve, which has its maximum near threshold and falls off rapidly with increasing energy. As ν decreases (increasing binding energy), the maximum moves to greater energies and the cross section decreases more slowly with increasing energy, until finally the $\nu=0.3$ curve approaches Lucovsky's δ-function model rather closely. In fact, in the limit of small ν, the normalized atomic cross section becomes independent of ν ($\equiv\alpha^{-1}$) and assumes the functional form $y^{3/2}/(1+y)^3$ appropriate to the δ-function model. Specifically, the δ-function model predicts the matrix element $|g|^2$ appearing in Eq. (59) to be

$$|g|^2=8y^{3/2}/(1+y)^4. \tag{60}$$

While the change in spectral shape between $\nu=0.3$ and the δ-function model $\nu \rightarrow 0.0$ seen in Fig. 6 appears to fit the established trend, the magnitude seems slightly anomalous. This probably is in part due to the uncertainty in specifying the correct normalization of the wave functions. The normalization of the QD functions in Eq. (3) is prescribed to force the functions to approach the correct magnitude for large r rather than to yield a normalization integral of unity, while the δ-function solutions are normalized to unity. Normalization of the QD functions to values different from unity is justified by the fact that the major contribution to optical integrals comes from moderately large values of r and that the wave functions are not required to be well defined near $r=0$. The apparent disparity between the results of the QDM and δ-function model is not sufficient to warrant trying to conform the two normalizations.

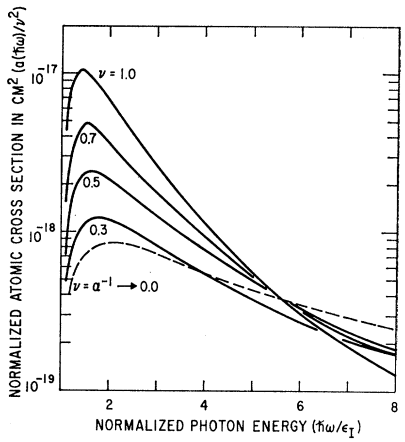

FIG. 6. Plot of normalized atomic cross section $a(\hbar\omega)/\nu^2$ versus normalized photon energy $\hbar\omega/\epsilon_I$ for different values of ν. The dashed $\nu \rightarrow 0.0$ curve is calculated from Lucovsky's δ-function model (Ref. 3).

VI. DISCUSSION

The effect of impurity binding energy on optical transitions is contained within the absorption cross section. Various optical properties such as absorption coefficient, radiative recombination rate, and lifetime are readily obtained from the calculated cross sections according to the prescriptions sketched in Sec. III. The major purpose of this work is to apply the QDM to calculate absorption cross sections for optical transitions involving impurities of arbitrary binding energies. Every effort is applied to put the results in a readily accessible form for interpreting experimental data.

Two cross sections are calculated: the impurity photo-ionization cross section (Fig. 3) and the band-impurity cross section (Fig. 2). Some general trends common to both calculations are of considerable experimental interest. From a comparison of Figs. 4 and 6 it is evident that as the impurity binding energy increases, the spectral dependence of the cross section becomes weaker and its magnitude decreases. Both of these trends make experimental observation of impurity-induced optical effects for deeper impurity centers more difficult; this is contrary to the intuitive argument that deeper centers should be easier to observe because they are further removed from the band edge.

Fourier relationships between $\mathbf{r}$ space and $\mathbf{k}$ space provide a unifying link to the general characteristics mentioned above. Both calculations (at least in the Born approximation) involve the quantity $|b(\gamma,\mathbf{k})|^2\epsilon^{1/2}$, where $b(\gamma,\mathbf{k})$ is the Fourier transform of $h(r)=r^\gamma e^{-\nu/\nu}$; for band-impurity transitions we have $0\geq\gamma(\equiv\nu-1)\geq-1$, and for photo-ionization transitions we have $1\geq\gamma(\equiv\nu)\geq0$ [compare Eqs. (29) and (54)]. The correlation in the spectral extent of $b(\gamma,\mathbf{k})$ with the compactness of $h(r)$ is apparent in Figs. 5 and 6.

Studies of photo-ionization processes of deep centers in semiconductors have been performed in sufficient detail to allow critical assessment of the applicablity of different theoretical models. Investigations of group-III impurities in silicon and the Hg center in germanium validate the QD model for impurities of arbitrary binding energies and the Lucovsky δ-function model for very deep impurities. Comparison of the present calculation with previous theoretical and experimental results indicates that the approximation of replacing the Coulomb continuum states with plane waves (while keeping QD ground-state functions) provides a quite simple working model which retains its sensitivity to the impurity binding energy. Indeed, appeal to experiment perhaps even favors the Born model over the full QD model. Certainly, when the in-

creased simplicity is also taken into account, use of the Born model can often be justified.

Recently, deep impurity centers have been recognized as potentially important in understanding optical properties of certain "ferroelectric-type" crystals. Some attempts to understand their influence have been attempted from a Lucovsky-like model.[20] Perhaps as these studies become more refined, the QD model will find application to these and other materials.

In the case of band-impurity transitions, much less experimental evidence concerning deep impurity centers exists with which to verify theoretical predictions. It has only been very recently that direct-gap semiconductor materials have been prepared of sufficient quality to give rise to emission lines which could be unambiguously identified as band-impurity transitions. Williams and Bebb[11] show that emission arising from conduction-band–acceptor transitions involving shallow acceptors in high-purity GaAs is accurately interpreted in terms of the hydrogenic model. In addition, band-edge absorption involving shallow impurities has been studied. It is hoped that similar studies on deeper centers will be performed.

Finally, we consider the realm of validity of the QD model. Basically the QDM is a technique for solving the usual effective-mass equation in a different and presumably improved approximation from the hydrogenic model. Thus, it clearly inherits all of the approximations embedded within the effective-mass theory itself. Of greatest concern is the requirement that the impurity envelope function remain slowly varying compared to the periodicity of the lattice. For very deep centers this condition is not well satisfied.[21] However, there is not yet any experimental evidence that violation of the slowly varying requirement detracts from the ability of the theory to yield accurate results. General experimental trends established for shallow to moderately deep impurities continue in a regular way to very deep centers, though their wave functions may extend only over a few lattice constants.

The QD theory does not *a priori* encompass defect centers associated with lattice defects, complex centers, or transition-metal ions, since these do not fall within the effective-mass formalism. In an earlier paper, the photo-ionization cross section of the manganese center in GaAs was shown to be in agreement with QD predictions. This comparison can be interpreted as fortuitous or considered as evidence that the transition-metal ion gives rise to Coulomb states in addition to the crystal field "*d* states."

ACKNOWLEDGMENTS

The author is grateful to Dr. E. W. Williams for supplying valuable experimental motivation for performing these calculations and to Professor J. S. Blakemore for several helpful discussions. Special thanks are due Dr. R. A. Chapman and Dr. E. W. Williams for numerous discussions and suggestions during the formative stages of the QD model for effective-mass impurities. Also, several discussions with Dr. G. Lucovsky concerning possible generalizations of the δ-function model and its connection with the QD model were of considerable value.

APPENDIX

For convenience we record an integral which is common to many QD calculations:

$$I(\gamma,k)=\int_0^\infty r^\gamma e^{-r\nu}e^{ikr}dr. \tag{A1}$$

The integral is the standard γ-function integral

$$I(\gamma,k)=\frac{\Gamma(\gamma+1)}{(1/\nu-ik)^{\gamma+1}}=\frac{\Gamma(\gamma+1)}{(1/\nu^2+k^2)^{(\gamma+1)/2}}\times e^{i(\gamma+1)\tan^{-1}\nu k}. \tag{A2}$$

In (A1), let $e^{ikr}=\cos kr+i\sin kr$; then we have

$$\begin{pmatrix}\mathrm{Im}\\ \mathrm{Re}\end{pmatrix}I(\gamma,k)=\frac{\nu^{\gamma+1}\Gamma(\gamma+1)}{(1+\nu^2k^2)^{(\gamma+1)/2}}\begin{pmatrix}\sin\theta\\ \cos\theta\end{pmatrix}, \tag{A3}$$

where $\theta=(\gamma+1)\tan^{-1}\nu k$.

[20] C. N. Berglund and H. J. Braun, Phys. Rev. **164**, 790 (1967).

[21] The need for the envelope function to encompass a large number of lattice constants arises from the approximation of replacing a summation over lattice points by an integral over all space to arrive at Eqs. (28) and (54) [cf., H. J. Zeiger, J. Phys. Chem. Solids **35**, 1657 (1964)]. The associated difficulty of describing wave functions in the immediate neighborhood of the impurity-ion case is bypassed because the optical integrals are insensitive to the nature of the wave functions at small r. This latter point is discussed in some detail by D. R. Bates and A. Damgaard, Phil. Trans. Roy. Soc. London **A242**, 101 (1949).